Theoretical analysis of the spatio-temporal structure of bone multicellular units

2010 IOP Conf. Ser.: Mater. Sci. Eng. 10 012132

(http://iopscience.iop.org/1757-899X/10/1/012132)

IOP Conf. Series: Materials Science and Engineering **10** (2010) 012132 doi:10.1088/1757-899X/10/1/012132

Theoretical analysis of the spatio-temporal structure of bone multicellular units

P R Buenzli[1], P Pivonka[1], B S Gardiner[1], D W Smith[1], C R Dunstan[2] and G R Mundy[3]

[1] Engineering Computational Biology Group, CSSE, Faculty of Engineering, Computing and Mathematics, The University of Western Australia, Australia
[2] Department of Biomedical Engineering, University of Sydney, NSW 2006, Australia
[3] Center for Bone Biology, Vanderbilt University, Nashville, 37232-0575, USA

E-mail: pascal.buenzli@uwa.edu.au

Abstract. Bone multicellular units (BMUs) maintain the viability of the skeletal tissue by coordinating locally the sequence of bone resorption and bone formation performed by cells of the osteoclastic and osteoblastic lineage. Understanding the emergence and the net bone balance of such structured microsystems out of the complex network of biochemical interactions between bone cells is fundamental for many bone-related diseases and the evaluation of fracture risk. Based on current experimental knowledge, we propose a spatio-temporal continuum model describing the interactions of osteoblastic and osteoclastic cells. We show that this model admits travelling-wave-like solutions with well-confined cell profiles upon specifying external conditions mimicking the environment encountered in cortical bone remodelling. The shapes of the various cell concentration profiles within this travelling structure are intrinsically linked to the parameters of the model such as differentiation, proliferation, and apoptosis rates of bone cells. The internal structure of BMUs is reproduced, allowing for experimental calibration. The spatial distribution of the key regulatory factors can also be exhibited, which in diseased states could give hints as to the biochemical agent most accountable for the disorder.

1. Introduction

The physiological process by which our bones are continuously renewed throughout our lifetime is commonly referred to as "bone remodelling" [1]. Old or damaged bone is removed by cells of osteoclastic lineage and replaced with new material by osteoblastic cells. This turnover of the skeletal tissue allows the repair of micro-cracks that accumulate as an effect of the repeated mechanical loading experienced by the bone structure. Besides mechanical function, bone remodelling is also crucial for calcium homeostasis by providing a quick release mechanism of the large amount of calcium stored in the bone matrix.

As first realised by Frost, the bone remodelling process is known to singularise spatio-temporally into "Bone Multicellular Units" (BMUs):[1] "*quanta*" of bone remodelling [2, 3, 4]. These entities, as revealed by histomorphometric sections, consist of teams of osteoclasts and osteoblasts working their way through the bone together in a self-consistent manner. Osteoclasts first resorb old bone upfront, opening a cutting cone in the bone matrix. This cavity is

[1] Sometimes also referred to as "Basic Multicellular Units", "Bone Metabolic Unit", or "Bone Remodelling Units".

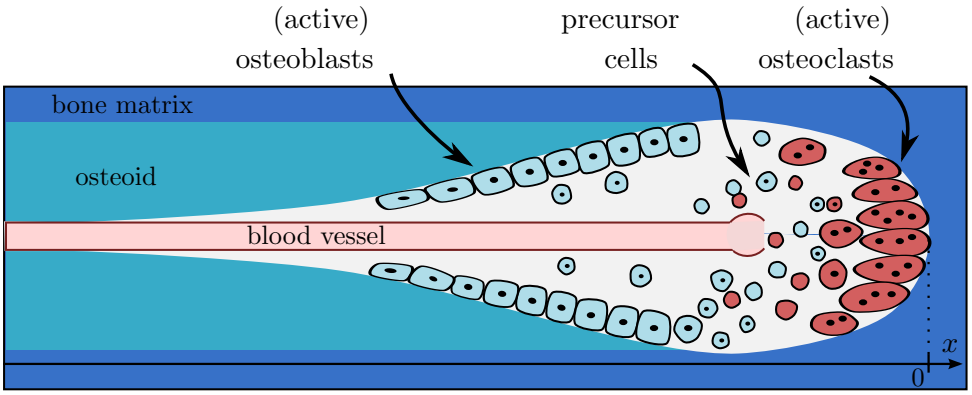

Figure 1. Schematic figure of the internal organisation of a (cortical) BMU. Osteoclasts resorb the bone matrix in the front while osteoblasts lay down osteoid (later to be mineralised) to refill the cavity in the back. The central blood vessel provides supply of precursor cells, as well as various nutrients.

subsequently closed in the back by osteoblasts laying down osteoid, later to be mineralised into new bone (see Figure 1, [5, 6, 7] and Refs. therein). The existence of such an organised microsystem is not entirely surprising biologically [4]. A tight localised coordination between bone resorption and bone formation is indeed necessary for a viable skeletal tissue. The bone structure and the specific shape of each bone need to be restituted within strict limits despite repeated resorption and formation. Not only is the overall bone loss/gain balance important, but also precisely the location of that resorption and reconstruction. Excess of resorption over formation can result in global but also local loss of bone mass and architecture, leading to fragility, vertebrae collapses and fractures, ultimately disabling the mobility of individuals having bone-related disorders such as osteoporosis.

Remodelling can be viewed as the sequence of two distinct processes. A first process recruits teams of bone-resorbing and bone-forming cells at specific sites of the bone in response to a certain stimulus. This stimulus activates or reduces remodelling on a per site basis and influences dramatically *when* and *where* a BMU is initiated. The second process is responsible for *how* the BMU evolves in the bone matrix; how the bone remodelling cells organise themselves locally into BMUs and regulate the crucial local balance between bone resorption and bone formation. This balance is coordinated by an intricate network of cell-cell interactions between variously-differentiated osteoclasts and osteoblasts. Numerous key regulatory factors in this network have been determined by Biologists in recent years and include systemic hormones, nerve signals, vascular agents, growth factors, chemokines, *etc.* (See [8, 9, 10] and Refs. therein.) However, it is not obvious how these interactions, usually thought of as occurring locally and simultaneously, organise osteoclasts and osteoblasts in the form of BMUs that present a clear spatial and temporal separation of these cells' activities. While the structure of BMUs is well understood on the descriptive level [5, 6, 7], how it is linked to these fundamental underlying mechanisms remains to be elucidated. In this contribution, we extend a previously-developed mathematical model of the bone remodelling biochemistry [10] to address these questions.

In recent years, several teams of researchers have elaborated mathematical and computational models of bone remodelling. The majority of these models focus on temporal aspects on the cellular level, *i.e.*, monitoring the temporal evolution of bone cells over time, while implementing a detailed biochemistry of interactions via rate equations [11, 9, 10]. Recently, Ryser *et al* have supplemented the temporal model [11] with a spatial component, addressing the important

question of interaction of locally expressed RANKL and soluble OPG [12, 13]. However, the organisation of the various cell distributions making the internal structure of a BMU is not investigated in detail. Cellular automata models have also been proposed to model resorption and formation on a per site basis [14], but key cellular biochemical processes relevant for a BMU's organisation are still missing in these models.

We present below a detailed spatio-temporal continuum model focusing on a single cortical BMU, extended from the cell-population model proposed by Pivonka *et al* [10]. We fully take into account osteoclastic and osteoblastic cells at various stages of differentiation along with the most important regulatory factors currently known to be involved in their interactions, such as Transforming Growth Factor β (TGF-β), Insuline-like Growth Factor (IGF), Parathyroid hormone (PTH) and the Receptor Activator Nuclear Factor $\kappa\beta$ axis consisting of the receptor RANK, the ligand RANKL and the decoy ligand osteoprotegrin (OPG).

2. Spatio-temporal model of cellular bone remodeling

In the confined biological environment of a BMU, the most important phenomena taking place are those of biochemical reactions and directed or diffusive motion of the various cells and regulatory factors. These phenomena are described in general by the mass continuity equations of the involved biochemical species [15, 16]. Let A denote such a species: a cell type, or any of the various regulatory agents (hormones, growth factors, paracrine factors, *etc*). Its associated mass balance equation is written as

$$\frac{\partial}{\partial t} n_A(\boldsymbol{r}, t) = -\boldsymbol{\nabla} \cdot \boldsymbol{J}_A(\boldsymbol{r}, t) + \sigma_A(\boldsymbol{r}, t). \tag{1}$$

In this equation, $n_A(\boldsymbol{r}, t)$ is the local concentration of A (number of entities A per unit volume) at point $\boldsymbol{r}$ in space and at time t, $\sigma_A(\boldsymbol{r}, t)$ is a local source/sink term, and $\boldsymbol{J}_A(\boldsymbol{r}, t)$ is the flux associated with the motion of As. Due to the several interactions occurring between the cells and factors, the mass-balance equations (1) written for all As are highly coupled. Couplings originating from the source/sink terms σ_A incorporate all the nonconservative mechanisms regulated by the presence of other agents, such as cell proliferation, differentiation, apoptosis, and factor binding/unbinding reactions. Couplings in the fluxes are differential in space and account for conservative modifications of the local concentrations as due to mass transport, *e.g.*, diffusion, chemotaxis, convection, *etc*.

We now specify the biochemical species and their couplings used in our model. After the initial process of BMU initiation, the BMU reaches a quasi-steady stage where its composing cells maintain a well-defined spatial structure travelling through the bone [5]. This stage is characteristic of the bone-remodelling process: bone-resorbing and bone-forming cells work in concert to turn over existing bone. Following the temporal model of bone remodelling proposed by Pivonka *et al* [10], we consider three osteoblastic and two osteoclastic cell types. "Uncommitted progenitor osteoblasts" (OB_us) denote a pool of mesenchymal stem cells that are capable of committing to the osteoblastic lineage. Following such commitment, they become "responding osteoblasts" or "preosteoblasts" (OB_ps). These preosteoblasts may further differentiate into "active osteoblasts" (OB_as) that are assumed to actively appose an osteoid seam to the remodelling cavity. "Precursor osteoclasts" (OC_ps), on the other hand, derive from hematopoietic progenitor cells and may differentiate into "active osteoclasts" (OC_as) that are capable of resorbing bone.

Regulatory actions on cellular differentiation from growth factors such as TGF-β/IGF (released from the dissolution of the bone matrix by OC_as), the RANK–RANKL–OPG signalling pathway, and the parathyroid hormone (PTH) are included, which effectively couples the system. A detailed description of these biochemical couplings and how they are transcribed mathematically in terms

of biochemical reaction rates can be found in [10] and will not be repeated here. The reaction rates of [10] correspond here precisely to the source/sink terms $\sigma_A(t)$ of (1).

The spatial organisation of the populations within the BMU highly depends on the fluxes $\boldsymbol{J}_A$s in (1). Generically, the flux of $\mathrm{OC_a}$s may be written $\boldsymbol{J}_{\mathrm{OC_a}} = n_{\mathrm{OC_a}}\,\boldsymbol{v}_{\mathrm{OC_a}}$, where $\boldsymbol{v}_{\mathrm{OC_a}}$ is the speed of $\mathrm{OC_a}$ cells with respect to the bone matrix. In the confined environment of an osteonal BMU, cell diffusion is limited and we may simply assume that $\mathrm{OC_a}$s travel at constant speed with a magnitude of the order of 20–40μm/day, matching the average speed $\boldsymbol{u}$ of a typical cortical BMU [6, 7]:

$$\boldsymbol{J}_{\mathrm{OC_a}} \approx n_{\mathrm{OC_a}}\,\boldsymbol{u}. \tag{2}$$

Active osteoblast are believed to lay down osteoid in the back of the BMU mainly radially, from the circumference of the cavity to the center. As this process occurs on much larger time scales compared to resorption, $\mathrm{OB_a}$s remain essentially stationary with respect to the bone along the BMU axis [17, 5, 6]. Disregarding cell diffusion again, and assuming that the preosteoblasts they derive from are not significantly moving longitudinally either, we set

$$\boldsymbol{J}_{\mathrm{OB_a}} \approx \boldsymbol{J}_{\mathrm{OB_p}} \approx \boldsymbol{0}. \tag{3}$$

In the temporal model [10], $\mathrm{OB_u}$ and $\mathrm{OC_p}$ precurseur cells were assumed to be provided in the system in the form of a large reservoir pool. In fact, as all cells eventually differentiate further or undergo apoptosis, a continual supply of these precursor cells needs to be provided to reach a quasi-steady state. In cortical remodelling, this supply is maintained by the growth of an internal blood vessel with the progression of the BMU. Similarly to [10], we assume here this supply to replenish $\mathrm{OB_u}$ and $\mathrm{OC_p}$ cells unlimitedly and fast enough in order that we can eliminate their dynamical description from the equations: their inhomogeneous densities instantaneously reach a stationary distribution loosely confined around the blood vessel extremity [5]. These concentrations thereby become external functions in the system of equations (1). Given that in the quasi-steady state, the vasculature progresses at the same rate $\boldsymbol{u}$ as the BMU front, we specify these functions as

$$n_P(\boldsymbol{r}, t) = n_P^{\mathrm{st}}(\boldsymbol{r} - \boldsymbol{u}t), \tag{4}$$

where $n_P^{\mathrm{st}}(\boldsymbol{r})$ ($P = \mathrm{OB_u}, \mathrm{OC_p}$) are the $\mathrm{OB_u}$ and $\mathrm{OC_p}$ stationary concentration profiles around the blood vessel extremity. Practically, n_P^{st} will be taken as Gaussian distributions.

Fast-binding hypothesis. A considerable simplification of the system of differential equations was obtained in [10] due to the separation of time scales between the fast reaction rates of ligands binding to their receptors on cells, and the slow cell responses (such as proliferation, differentiation and apoptosis). This allowed the rate equations corresponding to the various regulatory factors F of the system ($F = \text{TGF-}\beta/\text{IGF}, \text{RANKL}, \text{OPG}, \text{or PTH}$)[2] to be considered to reach their steady state immediately: $\frac{\partial}{\partial t} n_F \approx 0\ \forall t$. More precisely, this approximation holds when all the reaction rates involving F are large compared to the differentiation/apoptosis rates of cells. Let R_F be the slowest reaction rate (*e.g.*, in day^{-1}) to be found in σ_F. The fast-binding hypothesis states that R_F^{-1} is much smaller than the characteristic time involved in a variation of n_F: $\left|R_F^{-1}(\partial_t n_F)/n_F\right| \ll 1$. This effectively leads to

$$\sigma_F \approx 0 \tag{5}$$

[2] As $\mathrm{OC_p}$ cells are assumed to carry a fixed number of RANK receptors, the RANK concentration is directly proportional to that of $\mathrm{OC_p}$s, see Eq. (22).

from Eq. (1) when there is no flux term, as was used in [10] to derive Eqs. (11), (24), (25), (30) and (36). When a flux term is taken into account, the fast-binding hypothesis may still lead to (5) provided that the additional variation of n_F at $\boldsymbol{r}$ induced by spatial transport of F (such as due to diffusion for instance) is again small compared to R_F in the following sense:

$$R_F^{-1} \left| \partial_t n_F + \nabla \cdot \boldsymbol{J}_F \right| / n_F \ll 1. \tag{6}$$

We assume that the ranges of binding rates and migration/diffusion parameters pertaining to the regulatory factors F at stake in a BMU satisfy (6), and will thus use the simplified Eq. (5) instead of (1) for them.

Cell profiles in the comoving frame. In a fixed location of the bone about to be tunnelled by a travelling stationary BMU, one has a temporal picture in which several chronological phases can be distinguished according to the presence of certain types of cells: the resorption phase, the reversal phase, the formation phase and the mineralisation phase [5, 6, 7]. Accordingly, a temporal snapshot (picture) taken of a section of that portion of the bone (as shown, *e.g.*, in histomorphometric sections) reveals these same stages as spatially distinct zones: a resorption zone in the front of the unit, followed by a reversal, a formation, and a mineralisation zone (see *e.g.* [5, Fig. 2]). The same spatial structuring would be revealed to an observer travelling alongside the BMU in a co-moving frame. This entanglement of space and time is precisely the mark of travelling "bone cell waves" propagating with steady concentration profiles.

To follow the population of the biochemical species A along a propagating BMU, we consider a reference frame co-moving with the BMU at velocity $\boldsymbol{u}$. We assume the origin of this frame to coincide with the tip of the BMU's front and the x-axis to be directed along $\boldsymbol{u}$ (see Figure 1). Quantities observed in this new reference frame are denoted hereafter by the superscript "BMU". As $\boldsymbol{u}$ is assumed constant, they are obtained from the values observed in the bone frame by the well-known Galilean transformation:

$$n_A^{\mathrm{BMU}}(\boldsymbol{r}, t) = n_A(\boldsymbol{r} + \boldsymbol{u}t, t), \tag{7}$$
$$\boldsymbol{J}_A^{\mathrm{BMU}}(\boldsymbol{r}, t) = \boldsymbol{J}_A(\boldsymbol{r} + \boldsymbol{u}t, t) - n_A(\boldsymbol{r} + \boldsymbol{u}t, t)\boldsymbol{u}, \tag{8}$$
$$\sigma_A^{\mathrm{BMU}}(\boldsymbol{r}, t) = \sigma_A(\boldsymbol{r} + \boldsymbol{u}t, t). \tag{9}$$

As can be checked by differentiating (7) with respect to t on either side, this transformation leaves the form of the mass-balance equation (1) invariant: quantities superscripted with "BMU" also satisfy Eq. (1) (principle of Galilean relativity) [16]. The main difference that the BMU frame brings is an "apparent wind" flux term $-n_A^{\mathrm{BMU}}\boldsymbol{u}$ in $\boldsymbol{J}_A^{\mathrm{BMU}}$ (8) originating in the relative movement of that frame to bone and the velocity-addition law.

By definition, a quasi-steady state is reached by a travelling BMU if there is a time span during which all local quantities such as cell concentrations, fluxes, *etc.* become essentially independent of time in this co-moving frame. In other terms, $n_A^{\mathrm{BMU}}(\boldsymbol{r}, t)$ converges to a time-independent profile $n_A^{\mathrm{st}}(\boldsymbol{r})$ for times t such that $t_{\mathrm{initiation}} \ll t \ll t_{\mathrm{termination}}$:

$$n_A^{\mathrm{BMU}}(\boldsymbol{r}, t) \sim n_A^{\mathrm{st}}(\boldsymbol{r}). \tag{10}$$

Analogously, during the same window of time,

$$\boldsymbol{J}_A^{\mathrm{BMU}}(\boldsymbol{r}, t) \sim \boldsymbol{J}_A^{\mathrm{st}}(\boldsymbol{r}), \quad \sigma_A^{\mathrm{BMU}}(\boldsymbol{r}, t) \sim \sigma_A^{\mathrm{st}}(\boldsymbol{r}). \tag{11}$$

Taking the steady state limit (10)–(11) on the mass-balance equation in the co-moving frame, one obtains an ordinary differential equation for the spatial concentration profile n_A^{st} of the species A within the BMU:

$$\sigma_A^{\mathrm{st}}(\boldsymbol{r}) = \boldsymbol{\nabla} \cdot \boldsymbol{J}_A^{\mathrm{st}}(\boldsymbol{r}) = \boldsymbol{\nabla} \cdot \big[\boldsymbol{J}_A(\boldsymbol{r} + \boldsymbol{u}t, t) - n_A^{\mathrm{st}}(\boldsymbol{r})\boldsymbol{u} \big], \tag{12}$$

where $\boldsymbol{J}_A$ is the flux as seen in the bone frame and $\boldsymbol{J}_A(\boldsymbol{r}+\boldsymbol{u}t,t)$ is independent of time in the quasi-steady state. Note that by (8), the fast-binding hypothesis (6) leading to (5) holds in the BMU frame as well provided $\boldsymbol{u}$ is not too large. For the regulatory factors F that satisfy this condition, Eq. (12) thus reduces to

$$\sigma_F^{\mathrm{st}}(\boldsymbol{r}) = 0. \tag{13}$$

The unknowns to solve for in the set of coupled equations (12)–(13) written for all cells and factors are the steady-state density profiles $n_A^{\mathrm{st}}(\boldsymbol{r})$ in the BMU frame. Back in the bone frame, these densities take the form, by (7) and (10), of simple travelling waves whose undeforming shapes are the profiles $n_A^{\mathrm{st}}(\boldsymbol{r})$:

$$n_A(\boldsymbol{r},t) \sim n_A^{\mathrm{st}}(\boldsymbol{r}-\boldsymbol{u}t), \qquad t_{\mathrm{initiation}} \ll t \ll t_{\mathrm{termination}}. \tag{14}$$

Note that although osteoblastic cells are assumed to stay stationary with respect to the bone (see Eqs. (3)), wave-like solutions of their populations are still possible. The creation of cells "upstream" and destruction of cells "downstream" can produce travelling waves in the population distributions without stream on the cellular level. Having on the other hand conserved cells (never destroyed nor newly generated) but travelling individually at a fixed velocity starting from an initial distribution, the same travelling population distribution could be obtained.[3] However, we will see that in a system of interacting agents, these differences occasion dramatic changes in the resulting spatial structure of the wave profiles.

Solving the differential equations (12) requires supplementing them with appropriate boundary conditions. In the following, we write these equations explicitly for a one-dimensional model. For that situation, the boundary conditions only need to be specified at one point along the BMU and they will be considered along with the other parameters of the system.

One-dimensional model. As the spatial profiles in a BMU are more importantly structured along the x-axis we neglect variability of the densities in transversal cross-sections: $n_A^{\mathrm{st}}(\boldsymbol{r}) \approx n_A^{\mathrm{st}}(x)$. For ease of notation, we will denote from now on stationary profiles in the BMU frame $n_A^{\mathrm{st}}(x)$ by $A(x)$. Assuming that all regulatory molecules $F = \text{TGF-}\beta, \mathrm{PTH}, \mathrm{OPG}$ and RANKL concerned in the model satisfy the fast binding hypothesis (13), Eqs. (11), (25), (30) and (36) from [10] transfer in the BMU frame unchanged.[4] They give the expressions of $\text{TGF-}\beta, \mathrm{PTH}, \mathrm{OPG}$ and RANKL, respectively, in terms of the remaining dynamic variables of the system $\mathrm{OB_p}, \mathrm{OB_a}$ and $\mathrm{OC_a}$. For these slower-responding cells, we use instead Eq. (12) with fluxes specified by (2)–(3) and the same source/sink terms as found in the right hand side of Eqs. (4)–(6) of [10], leading to

$$-v\frac{\partial}{\partial x}\mathrm{OB_p}(x) = D_{\mathrm{OB_u}}\pi^{\mathrm{act}}\left(\frac{\text{TGF-}\beta(x)}{k_{\mathrm{OB_u}}^{\text{TGF-}\beta}}\right)\mathrm{OB_u}(x) - D_{\mathrm{OB_p}}\pi^{\mathrm{rep}}\left(\frac{\text{TGF-}\beta(x)}{k_{\mathrm{OB_p}}^{\text{TGF-}\beta}}\right)\mathrm{OB_p}(x), \tag{15}$$

$$-v\frac{\partial}{\partial x}\mathrm{OB_a}(x) = D_{\mathrm{OB_p}}\pi^{\mathrm{rep}}\left(\frac{\text{TGF-}\beta(x)}{k_{\mathrm{OB_p}}^{\text{TGF-}\beta}}\right)\mathrm{OB_p}(x) - A_{\mathrm{OC_a}}\mathrm{OB_a}(x), \tag{16}$$

$$D_{\mathrm{OC_p}}\pi^{\mathrm{act}}\left(\frac{\mathrm{RANKL}(x)}{k_{\mathrm{OC_p}}^{\mathrm{RANKL}}}\right)\mathrm{OC_p}(x) - A_{\mathrm{OC_a}}\pi^{\mathrm{act}}\left(\frac{\text{TGF-}\beta(x)}{k_{\mathrm{OC_a}}^{\text{TGF-}\beta}}\right)\mathrm{OC_a}(x) = 0. \tag{17}$$

In these equations, we have introduced the dimensionless universal activator and repressor "hill" functions

$$\pi^{\mathrm{act}}(\xi) = \frac{\xi}{1+\xi}, \qquad \pi^{\mathrm{rep}}(\xi) = 1 - \pi^{\mathrm{act}}(\xi) = \frac{1}{1+\xi}, \tag{18}$$

[3] A continuum spectrum of possibilities naturally exists between these two extreme situations.

[4] As in [10], IGF is assumed to act in pair with TGF-β.

respectively. Leaving out all external dosing terms of [10], the above functions allow us to rewrite the (unbound) ligand concentration profiles as[5]

$$\text{TGF-}\beta(x) = \frac{\alpha k_{\text{res}}}{\tilde{D}_{\text{TGF-}\beta}} \text{OC}_\text{a}(x), \tag{19}$$

$$\begin{aligned}\text{RANKL}(x) = {} & \frac{\beta_{\text{RANKL}}}{\tilde{D}_{\text{RANKL}}} \pi^{\text{rep}}(k_{\text{OPG}}^{\text{RANKL}} \text{OPG}(x) + k_{\text{RANK}}^{\text{RANKL}} \text{RANK}(x)) \\ & \times \pi^{\text{act}}\left(\frac{\tilde{D}_{\text{RANKL}}}{\beta_{\text{RANKL}}} N_{\text{OB}_\text{p}}^{\text{RANKL}} \text{OB}_\text{p}(x)\, \pi^{\text{act}}\left(\frac{\text{PTH}(x)}{k_{\text{OB,act}}^{\text{PTH}}}\right)\right)\end{aligned} \tag{20}$$

$$\text{OPG}(x) = \text{OPG}_{\max}\ \pi^{\text{act}}\left(\frac{\beta_{\text{OB}_\text{a}}^{\text{OPG}} \text{OB}_\text{a}(x)}{\text{OPG}_{\max} \tilde{D}_{\text{OPG}}} \pi^{\text{rep}}\left(\frac{\text{PTH}(x)}{k_{\text{OB,rep}}^{\text{PTH}}}\right)\right). \tag{21}$$

As the population of precursor osteclasts was assumed constant in [10], so was the concentration of RANK receptors. Here, OC_ps are distributed inhomogeneously in the system. We thus explicit the dependence of RANK upon OC_p by setting

$$\text{RANK}(x) = N_{\text{OC}_\text{p}}^{\text{RANK}} \text{OC}_\text{p}(x), \tag{22}$$

where $N_{\text{OC}_\text{p}}^{\text{RANK}} = 10^5$ is the number of RANK receptor per OC_p cell. The parathyroid hormone PTH is assumed to be provided homogeneously along the BMU at systemic levels: $\text{PTH}(x) \equiv \beta_{\text{PTH}}/\tilde{D}_{\text{PTH}} = 2.906$. The precursor cell density profiles within the BMU, $\text{OB}_\text{u}(x)$ and $\text{OC}_\text{p}(x)$, are assumed to be gaussianly distributed around the blood vessel extremity (set 350 μm behind the front of the BMU) with a standard deviation of the order of the reversal zone width (100 μm).

3. Results/discussion—density profiles within a bone multicellular unit

The resulting coupled system is expressed as the set of nonlinear differential equations specified in (15)–(22). These equations are solved numerically with standard stiff integrators (*e.g.* as provided by `Octave`, `Matlab` and/or `Mathematica`). In Figure 2, we show the various cell profiles obtained by solving these equations numerically for a certain set of parameter values. (The front of the BMU corresponds to the right of the figure, and its back to the left.) These profiles exhibit some of the main features expected from a cortical BMU, as explained hereafter.

We obtain well-defined profiles confined over a spatial range reasonably corresponding to that of a BMU (of the order of a few millimetres). These profiles define the shape of a multicellular wave front propagating into the bone at a constant velocity (towards the right in Figure 2), corresponding to a remodelling BMU. A clear spatial structure within this wave front is seen. Preosteoblasts and active osteoblasts are distinctly shifted towards the back of the BMU. Furthermore, the inversion of the relative number of OB_ps *vs* OB_as at around -700μm is clearly able to identify a "reversal zone" and a "formation zone" in the longitudinal axis of the BMU. This inversion is due to a relative shift of the corresponding cell population profiles. This shift can in fact be directly related to the parameters of the model and thus be used for its experimental calibration. Furthermore, the decaying tails of the OB_ps and OB_as can be linked to the elimination rate of OB_as (either by apoptosis or further differentiation) and the differentiation rate of OB_ps into OB_as. The experimental observation of such cell profiles from analyses of histological sections for exampe, could allow a direct determination of such cellular properties. More details on how to relate the observed shapes of the profiles to the parameters of the model from theoretical and numerical analyses will be developed in [18]. However, to

[5] In accordance with the conclusions of [10], we assume here that OPG is only produced by active osteoblasts and that RANKL is only expressed on precursor osteoblasts (corresponding to "Model Structure 2" of [10]).

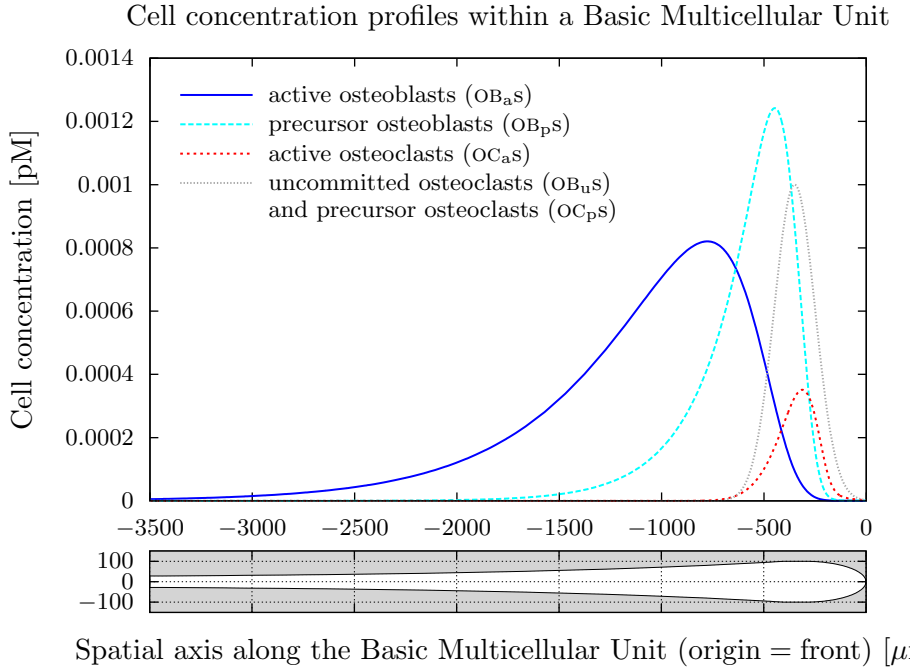

Figure 2. Density profiles of the bone cells in a cortical BMU obtained from the model. The inversion of OB_p and OB_a populations at around -700μm clearly outlines a transition between a reversal/resorption and a formation zones. A sketch (to scale) of a longitudinal section of a typical BMU cavity (with resorption and reversal zone lengths taken as 300μm and 100μm respectively) is aligned with the profile plots for convenience.

give an idea of the importance of the flux term contributions in the emergence of such spatial structuring, Figure 3 depicts the cellular profiles obtained from a situation in which all cellular fluxes are taken proportional to the average velocity of the BMU, as in (2). In that case, all the cell populations fall within the same region around the precursor cell source.

The resorption cone of the BMU, on the other hand, is not represented very well by the current settings of the model: in particular, there is no inversion of the populations of OC_as over OC_ps in the front of the BMU. In fact, in our model, OC_as are produced from OC_ps around the middle of the reversal zone ($\approx -350\mu$m) and have not been given mechanisms allowing them to distance themselves from their progenitors (such as chemotactic signals towards the bone surface). It is interesting to acknowledge that the bone remodelling biochemistry implicated in our model, whilst sufficient to explain generic features of the bone-formation-related part of the BMU, is not satisfactory in explaining the spatial structure of the cutting cone of the BMU, which hints at missing biochemical signalling components.

4. Concluding Remarks

We have developed a continuum spatio-temporal mathematical model to study cell profiles in a cortical BMU. This model is based on general mass-balance equations. Nonconservative production or elimination of biochemical components in these equations are set in accordance with the biochemistry currently believed to play the most important role in bone remodelling.

We have obtained solutions of our equations in the form of well-defined profiles confined in a small region of space, and travelling at constant velocity in the bone. These profiles exhibit a spatial structure along the longitudinal axis corresponding to the known organisation of bone

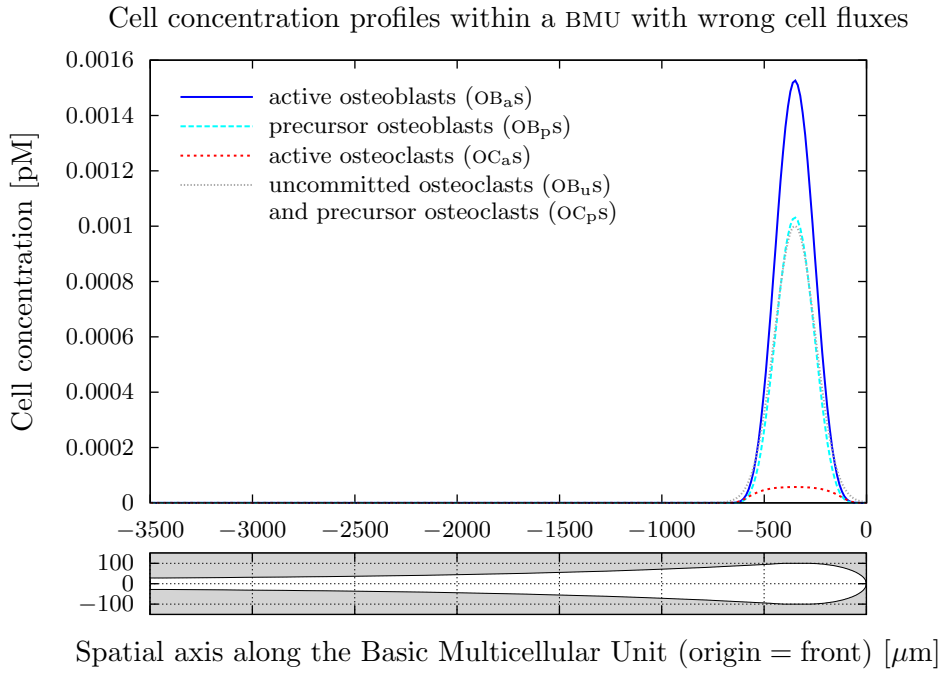

Figure 3. Density profiles obtained when the fluxes are taken $\boldsymbol{J}_A = n_A \boldsymbol{u}$ for all cells $A = \mathrm{OB_p}, \mathrm{OB_a}, \mathrm{OC_a}$. All other parameters are otherwise taken as in Figure (2). The typical spatial organisation of the bone cells in a BMU is not reproduced in this case. These profiles are in clear mismatch with the typical shape of the BMU cavity sketched below to scale.

cells in BMUs. The specification of the cell fluxes, describing chemotaxis, migration, diffusion *etc.*, appears to be crucial in explaining the spatial structure of the BMUs. In particular, our theoretical results confirm that osteoblasts ($\mathrm{OB_p}$, $\mathrm{OB_a}$) do not move independently in the cavity, but are rather quasi-stationary with respect to the bone.

The biochemical interactions considered between the various osteoclastic and osteoblastic cells of our model therefore explain the possibility of the emergence and stability of organised, spatially structured, groups of cells in the form of BMUs. While the bone-formation zone of the BMU is well described by the implemented biochemistry, some inconsistencies of the profile shapes at the front of the BMU indicate that a mechanism is missing in the model; namely, one that allows active osteoclasts to be moved to the front of their progenitor cells. This will be the subject of future work.

Nevertheless, the model allows to address several interesting points: cellular elimination rates and differentiation rates could be directly inferred from the shapes of the concentration profiles [18]. This provides a convenient way of determining such temporal cell properties from the observation of spatial profiles at a single moment in time (histological snapshot), allowing convenient experimental calibration of the model. Furthermore, as the bone cells in a moving BMU interact by means of several regulatory factors, the spatial distribution of these cells along the BMU reflects that of the factors. A local concentration of these molecules could thus be inferred from the easier observation of the spatial cellular profiles. For example, TGF-β and (free, $\mathrm{OB_p}$-bound) RANKL turn out to be very localised in the reversal/resorption zone of a BMU in our simulations. For RANKL, this occurs in spite of a sparser $\mathrm{OB_p}$ population in these zones and is explained by a corresponding depletion of OPG, which is linked to active osteoblasts in our model. The correspondences between cell and factor profiles will be examined further in [18].

Acknowledgments
This work is supported by the Australian Research Council grant DP089466.

References
[1] Frost H M 1973 *Bone Remodeling and its Relationship to Metabolic Bone Disease* (Boston: CC Thomas)
[2] Frost H M 1964 Dynamics of bone remodeling. In *Bone Biodynamics*, ed H M Frost (Boston: Little, Brown & Co.)
[3] Parfitt A M 1979 Quantum concept of bone remodeling and turnover: implications for the pathogenesis of osteoporosis. *Calcif. Tissue Int.* **28** 1–5
[4] Parfitt A M 1984 The cellular basis of bone remodeling: the quantum concept reexamined in light of recent advances in the cell biology of bone. *Calcif. Tissue Int.* **36** S37–S45
[5] Parfitt A M 1994 Osteonal and hemi-osteonal remodeling: the spatial and temporal framework for signal traffic in adult human bone. *J. Cell. Biochem.* **55** 273–286
[6] Martin R B, Burr D B and Sharkey N A 1998 *Skeletal Tissue Mechanics* (New York: Springer)
[7] ed S C Cowin 2001 *Bone Mechanics Handbook* 2$^{\text{nd}}$Ed (Boca Raton: CRC Press)
[8] Martin T J 2004 Paracrine regulation of osteoclast formation and activity: milestones in discovery *J. Musculoskel. Neuron. Interact.* **4** 243–253
[9] Lemaire V, Tobin F L, Greller L D, Cho C R and Suva L J 2004 Modeling the interactions between osteoblast and osteoclast activities in bone remodeling *J. Theor. Biol.* **29** 293–309
[10] Pivonka P, Zimak J, Smith D W, Gardiner B S, Dunstan C R, Sims N A, Martin T J and Mundy G R 2008 Model structure and control of bone remodeling: a theoretical study. Bone **43**:249–263
[11] Komarova S V, Smith R J, Dixon S J, Sims S M and Wahl L M 2003 Mathematical model predicts a critical role for osteoclast autocrine regulation in the control of bone remodeling *J. Theor. Biol.* **229** 293–309
[12] Ryser M D, Nigam N and Komarova S V 2009 Mathematical modeling of spatio-temporal dynamics of a single bone multicellular unit. *J. Bone Miner. Res.* **24**
[13] Ryser M D, Komarova S V and Nigam N 2010. The cellular dynamics of bone remodelling: a mathematical model. *SIAM J. Appl. Math.* **70** 1899–1921
[14] van Oers R F M, Ruimerman R, Tanck E, Hilbers P A J and Huiskes R 2008 A unified theory for osteonal and hemi-osteonal remodeling *Bone* **42** 250–259
[15] Bird R B, Stewart W E and Lightfoot E N 2002 *Transport Phenomena* 2$^{\text{nd}}$Ed (New York: Wiley)
[16] Scheurer P B and Stueckelberg de Breidenbach E C G 1974 *Thermocinétique Phénoménologique Galiléenne* (Basel: Birkhäuser)
[17] Jarowski J F G and Hooper C 1980. Study of cell kinetics within evolving secondary haversian systems. *J. Anat. London* **131**:91–102
[18] Buenzli P R, Pivonka P, Smith D W, and Dunstan C R. Cell distributions in a bone multicellular unit: a spatio-temporal model. In preparation (2010).